JOURNAL OF COMPUTATIONAL PHYSICS **145,** 538–554 (1998)
ARTICLE NO. CP986038

Complex Solution to Nonideal Contaminant Transport Through Porous Media

Giuseppe Gambolati and Giorgio Pini

Dip. di Metodi e Modelli Matematici per le Scienze Applicate, University of Padua, Italy

Received October 30, 1997; revised May 8, 1998

Nonideal or nonequilibrium transport through porous media is described by a convection-diffusion equation coupled to a first order kinetics accounting for mass transfer between the solid and the fluid phases. The overall mathematical model may be formulated using an integro-differential approach and very effectively Laplace transformed with complex parameters p_k, $k = 0, 1, \ldots, 2M+1$. Solution in Laplace space may be addressed by finite elements (FE). The resulting complex valued FE equations can be solved with either a complex or an equivalent real arithmetic operating on a problem twice as large as the original one. For both approaches preconditioned projection (or conjugate gradient-like) methods are used. Particularly difficult problems with high Peclet numbers are investigated as well. The results from three representative test cases totalling up to 15,000 equations show that the complex solution approach is superior to the real approach by up to almost two orders of magnitude, depending on the problem. It is also shown that while the solver performance vs p_k is stable in complex arithmetic, this does not hold true for the solver in real arithmetic, and an argument based on the quality of preconditioning is offered to account for the observed different computational behavior.

1. INTRODUCTION

The transport of reactive contaminants in sorbing porous media characterized by intra-aggregate diffusion or chemical processes which do not satisfy the local equilibrium can be mathematically described by the so-called two-site, or two-domain or dual porosity model [5, 33, 6]. When a first-order kinetic relationship is used to represent the transfer of mass between domains, the model can be expressed as a modified advection-dispersion equation describing general transport coupled to a first order ordinary differential equation accounting for mass transfer. Different approaches may be used to solve the resulting system [14], including: (1) simultaneously solving the coupled transport and kinetic equation [16]; (2) discretizing and algebraically solving the mass transfer equation and substituting it into the transport equation [24]; (3) solving the mass transfer equation analytically and

0021-9991/98 $25.00

substituting the integral solution into the transport equation to obtain a single integro-differential equation [15]; (4) solving the system in Laplace space and back transforming the solution into the time domain [19]. In the latter approach, called FELT (Finite Element Laplace Transform), a Laplace transformation is applied to the integro-differential equation, eliminating the time variable and exploiting the simple form of the convolution integral in Laplace space. The transformed equation is solved by finite elements, and an inversion algorithm is applied to recover the solution to the time domain [29, 30].

The finite element solution in Laplace space must be obtained for $2(M+1)$ values of the Laplace parameter p_k ($k = 0, 1, \ldots, 2M+1$). Typical values for M are in the range 15–25 with the need for using a higher value ($M \sim 40$) only in particularly difficult advection dominated problems [19, 14]. Parameter p_k influences both the coefficient matrix and the known vector so for each k-value a distinct finite element set of unsymmetric equations must be solved. To preserve stability of the inversion algorithm complex p_k are recommended. Hence complex systems are obtained in Laplace space.

The solution to these complex systems can be achieved by two different approaches. In the first approach, which is followed in [19, 14], the N original complex equations are transformed into $2N$ real equations with the real and imaginary solution parts forming a single real vector of unknowns. This approach requires solving for each Laplace parameter p_k a discrete problem twice as large as the corresponding finite element problem. In the second approach the complex p_k-system is solved by a complex solver with a complex arithmetic, thus preserving the original system dimension N. In general the numerical problem may be difficult to solve when advection dominates over dispersion, i.e., for large Peclet numbers Pe (usually for $Pe > 2$).

In both the real and the complex approach iterative solvers belonging to the class of conjugate gradient-like methods are used, in particular the schemes TFQMR (Transpose Free Quasi Minimal Residual) [13, 27] and Bi-CGSTAB (Bi-Conjugate Gradient Stabilized) [31] which turn out to be the most reliable, robust, and efficient solvers for real unsymmetric problems of the type discussed in the present paper [18]. To accelerate convergence TFQMR and Bi-CGSTAB have to be preconditioned. Although several variants of the incomplete factorization algorithm with controlled fill-in are available and have been much studied in the solution of real advection-diffusion systems [18], use will be made here of the simple preconditioner ILU(0) [25, 22, 28] where the incomplete triangular factor L and U have the same sparsity pattern as the lower and upper part of the finite element matrix, respectively.

While an extensive literature on the iterative conjugate gradient solution of real coefficient systems exists, the solution to complex sparse systems by these methods is addressed in a very limited number of papers. A theoretical outline may be found in [12, 21]. For a few symmetric non-Hermitian applications in electrodynamics the reader may refer to [7, 4]. Numerical studies in elasto-dynamics and hydrodynamics involving complex unsymmetric matrices are provided in [2, 9]. The present analysis is an additional contribution to the solution of complex equations with reference to the FELT method as it applies to the solution of nonequilibrium contaminant transport through porous media.

The outline of the paper is as follows. We first review the FELT algorithm and comment on the resulting complex finite element systems. The iterative solvers TFQMR and Bi-CGSTAB are briefly described along with the preconditioner used in the numerical tests. Then the most salient results of three numerical experiments with N in the range 1000–15,000 are shown and discussed. The different behavior of the complex and real solvers vs the Laplace parameter p_k is investigated in detail, and an argument is given to account for

the high sensitivity to the Laplace parameter p_k of the real solver convergence. A set of conclusive remarks and recommendations is finally issued.

2. COMPLEX SOLUTION APPROACH

The general equations describing the linear dual-porosity model in a porous media are [15]

$$\frac{\partial}{\partial x_i}\left(D_{ij}\frac{\partial c_m}{\partial x_j}\right) - v_i\frac{\partial c_m}{\partial x_i} = T_m\frac{\partial c_m}{\partial t} + T_{im}\frac{\partial c_{im}}{\partial t} + \lambda(T_m c_m + T_{im}c_{im}) + q(c_m - c^*) - f \tag{1a}$$

$$T_{im}\frac{\partial c_{im}}{\partial t} = \alpha(c_m - c_{im}) - \lambda T_{im}c_{im}, \tag{1b}$$

where x_i is the ith Cartesian coordinate, t is time, c_m and c_{im} are the concentrations of the dissolved constituent in the mobile and immobile water regions, λ is the linear decay constant, α is the mass transfer coefficient controlling the diffusion process between the mobile and immobile water regions, q represents distributed source/sink terms (volumetric flow rate per unit volume), c^* is the concentration of the solute injected or withdrawn with the fluid source or sink, f is the distributed mass rate of the solute per unit volume, and T_m and T_{im} are modified retardation coefficients. The dispersion coefficient D_{ij} is written using Bear's relationship [3] which involves the longitudinal and transverse dispersivities α_L and α_T; v_i is the Darcy velocity. Equation (1a) holds in a 2-D or 3-D space, with the indicial notation denoting summation accordingly.

Integrating Eq. (1b) analytically, assuming $c_{im}(x_i, t = 0) = 0$, and substituting the result into (1a) leads to an integro-differential equation for the mobile region concentration [15],

$$\frac{\partial}{\partial x_i}\left(D_{ij}\frac{\partial c_m}{\partial x_j}\right) - v_i\frac{\partial c_m}{\partial x_j} = T_m\frac{\partial c_m}{\partial t} + (\alpha + \lambda T_m + q)c_m - \alpha\beta\int_0^t e^{-(\beta+\lambda)(t-\tau)}c_m(\tau)\,d\tau - (qc^* + f), \tag{2}$$

where $\beta = \alpha/T_{im}$.

Equation (2) forms the basis for the integro-differential approach of the dual-porosity model.

If p_k is the complex-valued Laplace parameter then applying the Laplace transform to Eq. (2) leads to the equation [19, 14]

$$\frac{\partial}{\partial x_i}\left(D_{ij}\frac{\partial \bar{c}_m}{\partial x_j}\right) - v_i\frac{\partial \bar{c}_m}{\partial x_i} = \left[T_m(p_k + \lambda) + \frac{\alpha T_{im}(p_k + \lambda)}{T_{im}(p_k + \lambda) + \alpha}\right]\bar{c}_m + q(\bar{c}_m - \bar{c}^*) - \bar{f} - T_m c_m(x_i, t = 0), \tag{3}$$

where the bar denotes a Laplace transformed quantity. Equation (3) is a time independent transport equation with a complex valued coefficient before $\bar{c}_m$ to be solved in space, the time being removed by the Laplace transformation. Its solution is a function of the Laplace parameter p_k. Equation (3) together with the transformed boundary conditions (which may be of Dirichlet, Neumann, and Cauchy type) is solved in Laplace space by the finite element (FE) method using standard triangular or tetrahedral finite elements with linear basis functions [15, 17]. Use is made of the classic Galerkin formulation with the

Green lemma applied to the diffusive component of Eq. (3) and no upwind of the convective term. For a description of this approach which is well known, and the construction of the related stiffness and convective matrices and the complex valued capacity matrix, the reader may refer to widespread textbooks such as [32, 1, 34]. If N is the size of the FE grid, the solution to Eq. (3) yields an $N \times N$ algebraic system

$$G\bar{\boldsymbol{c}} = \boldsymbol{b}, \tag{4}$$

where $G = A + B + F + S$ with A and B the standard real stiffness and advection matrices, F a real matrix arising from the Cauchy type boundary conditions, and S a complex-valued capacity matrix arising from the term which involves in Eq. (3) the complex Laplace parameter p_k. The complex-valued vector $\boldsymbol{b}$ accounts for the transformed boundary conditions together with source and sink terms. Note that matrix G is unsymmetric because of the advection matrix B. System (4) represents a set of linear algebraic equations in the complex space, with G a function of p_k through S. Consider the coefficient which multiplies $\bar{c}_m$ in Eq. (3) and is used to form S. Define p_k as

$$p_k = p_0 + ik\pi/T, \qquad k = 0, 1, 2, \ldots, 2M + 1, \tag{5}$$

where $i = \sqrt{-1}$, $T = 0.8t_{max}$, t_{max} is the maximum simulation time [8], and $p_0 = -\ln(\epsilon)/2T$, where ϵ is the absolute error term. For a selection of these parameters the reader should refer to [8].

Separating the real part from the imaginary part in Eq. (3) and using (5) yield

$$T_m(p_k + \lambda) + \frac{\alpha T_{im}(p_k + \lambda)}{T_{im}(p_k + \lambda) + \alpha} = \frac{Z_k}{\Upsilon_k} + i\left(\frac{k\pi}{T}\right)\left(T_m + \frac{\alpha^2 T_{im}}{\Upsilon_k}\right), \tag{6}$$

where

$$\Upsilon_k = [T_{im}(p_0 + \lambda) + \alpha]^2 + \left(T_{im}\frac{k\pi}{T}\right)^2$$

$$Z_k = (p_0 + \lambda)\{T_m\Upsilon_k + \alpha T_{im}[T_{im}(p_0 + \lambda) + \alpha]\} + \alpha T_{im}^2\left(\frac{k\pi}{T}\right)^2.$$

The relative importance of the imaginary part is measured by the ratio

$$R_k = \frac{(k\pi/T)\left(T_m\Upsilon_k + \alpha^2 T_{im}\right)}{Z_k}$$

$$= \frac{(k\pi/T)\left(T_m + \alpha^2 T_{im}/\Upsilon_k\right)}{(p_0 + \lambda)\{T_m + (\alpha T_{im}/\Upsilon_k)[T_{im}(p_0 + \lambda) + \alpha]\} + \alpha\left(T_{im}^2/\Upsilon_k\right)(k\pi/T)^2}. \tag{7}$$

Note that for a given problem R_k is a growing function of k for k larger than a threshold value, and asymptotically grows linearly with k. Hence for k sufficiently large the capacity matrix S approaches a pure imaginary matrix. Setting $\lambda = 0$ for large k-values leads to

$$R_k = \frac{2\pi k}{-\ln\epsilon + 2\alpha(T/T_m)} \tag{8}$$

increasing linearly with k.

If we denote by $\bar{\mathbf{c}}_{m,R}$ and $\bar{\mathbf{c}}_{m,I}$ the real and imaginary part of $\bar{\mathbf{c}}_m$, the set of complex-valued equations (4) can be transformed into an equivalent set of real equations twice as large,

$$\begin{pmatrix} G_R & -S_I \\ S_I & G_R \end{pmatrix} \begin{pmatrix} \bar{\mathbf{c}}_{m,R} \\ \bar{\mathbf{c}}_{m,I} \end{pmatrix} = \begin{pmatrix} \mathbf{b}_R \\ \mathbf{b}_I \end{pmatrix}, \tag{9}$$

where $G_R = A + B + F + S_R$, S_R and S_I being the real and imaginary symmetric part of S, and $\mathbf{b}_R$ and $\mathbf{b}_I$ the real and imaginary part of the right hand side vector containing boundary conditions and source/sink terms. Solving (4) with complex arithmetic is mathematically equivalent to solving (9) with real arithmetic. However, computationally the equivalence does not hold as the numerical operations required by the two approaches are different from both a qualitative and a quantitative viewpoint irrespective of the influence of round-off errors on the iterates. This study is aimed at investigating and comparing the computational performance of TFQMR and Bi-CGSTAB when they are used in the solution of Eqs. (4) and (9).

When $\bar{c}_m(p_k)$, $k = 0, 1, \ldots, 2M+1$, is available, the back transformed concentration $c_{j,k}$ at node j is computed as

$$c_j(t) \approx \frac{e^{p_0 t}}{T} \left\{ \frac{1}{2} \bar{c}_{j,0} + \sum_{k=1}^{2M+1} \left[\mathrm{Re}(\bar{c}_{j,k}) \cos\left(\frac{k\pi t}{T}\right) - \mathrm{Im}(\bar{c}_{j,k}) \sin\left(\frac{k\pi t}{T}\right) \right] \right\}. \tag{10}$$

The value of M has to be set large enough to ensure convergence of the summation in (10) to the correct concentration $c_j(t)$. In practice M is chosen in the range 5 to 40 since cancellation errors may become dominant for M larger than 40 [10]. Selection of an appropriate M is problem dependent. For instance, steep gradients in advection dominated analyses call for M in the upper range. The parameter t_{max} must also be selected carefully. If the solution is sought at a time value $t \ll t_{max}$ an oscillating solution may be observed despite using a large M value in (10) [19]. In this case it may be necessary to perform the simulation with a properly reduced t_{max}.

3. PRECONDITIONED PROJECTION METHODS

In this section we summarize the TFQMR scheme for the solution of both Eqs. (4) and (9). The theoretical development of the algorithm may found in [13, 27] while an extensive numerical study of the TFQMR performance for real equations has been contributed in [18]. For Bi-CGSTAB the reader is referred to [31].

We consider the system of linear equations

$$A\boldsymbol{x} = \boldsymbol{b}, \tag{11}$$

where matrix A is non-symmetric, possibly complex and sparse, with dimension N. As usual we set $\boldsymbol{x}^+\boldsymbol{y} = \sum_{i=1,n} \bar{x}_i y_i$ and $\|\boldsymbol{x}\| = \sqrt{\mathbf{x}^+\mathbf{x}}$

The TFQMR algorithm with general weights may be described by the following recursive relationships:

1. Start:
   (a) Choose $\boldsymbol{x}_0 \in \mathbb{C}^N$;
   (b) Set $\boldsymbol{p}_0 = \boldsymbol{u}_0 = \boldsymbol{r}_0^{CGS} = \boldsymbol{r}_0 = \boldsymbol{b} - A\boldsymbol{x}_0, \boldsymbol{v}_0 = A\boldsymbol{p}_0,\ \boldsymbol{d}_0 = \boldsymbol{0}$;
   $\tau_0 = \omega_1 = \left\|\boldsymbol{r}_0^{CGS}\right\|, \theta_0 = 0, \eta_0 = 0$;
   (c) choose $\tilde{\mathbf{r}}_0$ such that $\rho_0 = \tilde{\mathbf{r}}_0^+ \mathbf{r}_0 \neq 0$ (e.g., $\tilde{\mathbf{r}}_0 = \mathbf{r}_0$);
2. For $j = 1, 2, \ldots$ do:
   (a) set $\sigma_{j-1} = \tilde{\mathbf{r}}_0^+ \boldsymbol{v}_{j-1}, \alpha_{j-1} = \rho_{j-1}/\sigma_{j-1}$;
   $\boldsymbol{q}_j = \boldsymbol{u}_{j-1} - \alpha_{j-1}\boldsymbol{v}_{j-1}$
   $\boldsymbol{r}_j^{CGS} = \boldsymbol{r}_{j-1}^{CGS} - \alpha_{j-1}A(\boldsymbol{u}_{j-1} + \boldsymbol{q}_j)$
   (b) For $m = 2j-1, 2j$ do:

$$\text{set } \omega_{m+1} = \begin{cases} \sqrt{\left\|\boldsymbol{r}_{j-1}^{CGS}\right\|\left\|\boldsymbol{r}_j^{CGS}\right\|}, & \text{if } m = 2j-1, \\ \left\|\boldsymbol{r}_j^{CGS}\right\|, & \text{if } m = 2j. \end{cases}$$

   $\theta_m = \omega_{m+1}/\tau_{m-1}, c_m = 1/\sqrt{1+\theta_m^2}$;
   $\tau_m = \tau_{m-1}\theta_m c_m, \eta_m = c_m^2 \alpha_{j-1}$;
   $\boldsymbol{d}_m = \boldsymbol{y}_m + \left(\theta_{m-1}^2 \eta_{m-1}/\alpha_{j-1}\right)\boldsymbol{d}_{m-1}$;

$$\text{where } \boldsymbol{y}_m = \begin{cases} \boldsymbol{u}_{j-1}, & \text{if } m = 2j-1, \\ \boldsymbol{q}_j, & \text{if } m = 2j. \end{cases}$$

   $\boldsymbol{x}_m = \boldsymbol{x}_{m-1} + \eta_m \boldsymbol{d}_m$
   If $\boldsymbol{x}_m$ has converged: stop;
   (c) set $\rho_j = \tilde{\mathbf{r}}_0^+ \mathbf{r}_j^{CGS}, \beta_j = \rho_j/\rho_{j-1}$;
   $\boldsymbol{u}_j = \mathbf{r}_j^{CGS} + \beta_j \boldsymbol{q}_j$;
   $\boldsymbol{p}_j = \boldsymbol{u}_j + \beta_j(\boldsymbol{q}_j + \beta_j \boldsymbol{p}_{j-1})$;
   $\boldsymbol{v}_j = A\boldsymbol{p}_j$

The stopping criterion is written as

$$\frac{\|\boldsymbol{r}_m\|}{\|\boldsymbol{r}_0\|} \leq \frac{\sqrt{m+1}\,\tau_m}{\|\boldsymbol{r}_0\|} \leq \epsilon_1.$$

In the numerical experiments that follow we use a zero initial guess with an exit tolerance $\epsilon_1 = 10^{-15}$. As was mentioned in the Introduction both TFQMR and Bi-CGSTAB are preconditioned with ILU(0).

4. COMPUTATIONAL PERFORMANCE SOLVER IN COMPLEX AND REAL ARITHMETIC

Three sample problems are used to address the computational performance of the complex solvers. For the Laplace inversion, to ensure convergence of the *epsilon* algorithm we adopt a value of $\epsilon = 10^{-15}$ (see [26]) and $M = 7, 15, 31$ with $r = 2(M+1) = 16, 32, 64$. The runs are performed on an IBM RISC 6000/390, and the CPU times are given in seconds.

4.1. *Sample Problem* 1: *Transport in a Saturated Soil Slab*

Nonequilibrium transport in a two-dimensional rectangular slab is considered in this example. The problem is adapted from [16] to include nonequilibrium sorption. A uniform

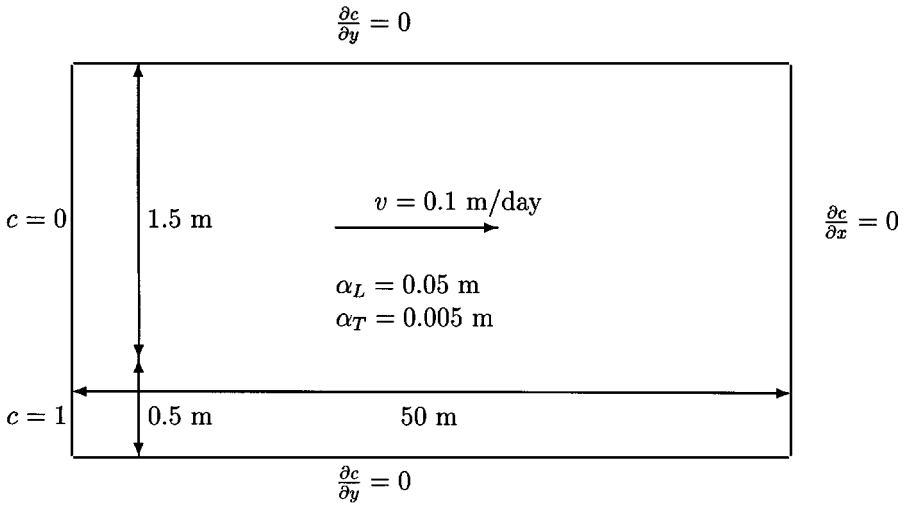

FIG. 1. Schematic description of the domain for Problem 1.

velocity field is assumed over the whole domain (Fig. 1). The horizontal and vertical mesh spacings Δx and Δy are 1 and 0.1 m, respectively. This results in a uniform triangulation with 1071 nodes. The linear real systems (9) have a dimension $2N = 2142$ and a number of matrix nonzero elements equal to 7211. The longitudinal and transverse dispersivities are $\alpha_L = 0.05$ m and $\alpha_T = 0.005$ m, with a grid Peclet number equal to $Pe = \Delta x/\alpha_L = 20$. The retardation factors and the porosities in the mobile and immobile zones are $T_m = 0.4$ and $T_{im} = 0.2$. The time t_{max} is equal to 10 days. The mass transfer coefficient α is taken equal to 0.05 day^{-1} while the decay constant λ is set to zero. With these parameter values the factor R_k takes on the expression

$$R_k = \frac{7.81\,10^{-5}k + 2.87\,10^{-7}k^3}{4.71\,10^{-4} + 2.95\,10^{-6}k^2}.$$

Note that R_k is a growing function of k over the entire k range, as is shown in the leftmost column of Table I.

Table II shows the cumulative number IT of iterations, the average cost per iteration IC, and the overall CPU time CPUT required by TFQMR and Bi-CGSTAB to solve the $r = 2(M + 1)$ real systems (9). Table III gives similar results when the complex arithmetic

TABLE I
Behavior of R_k in the Various Sample Problems

k	Problem 1	Problem 2	Problem 3a–3b	Problem 3c–3d
1	0.17	0.16	0.17	0.18
2	0.33	0.32	0.34	0.36
3	0.49	0.48	0.51	0.55
4	0.64	0.64	0.66	0.73
5	0.78	0.85	0.82	0.91
15	1.89	2.34	1.80	2.73
31	3.32	4.81	1.93	5.64
63	6.30	9.77	1.50	11.46

TABLE II
Performance of TFQMR (*T*) and Bi-CGSTAB (*B*) in the Solution of the Real Systems (9) for Sample Problem 1

r	Solver	IT	IC(s)	CPUT(s)
16	T	200	0.04	7.5
16	B	167	0.04	6.6
32	T	462	0.04	17.0
32	B	377	0.04	14.4
64	T	1158	0.04	40.8
64	B	936	0.04	34.2

is used for Eqs. (4), in addition to the speed-up S_s, defined as the ratio between the CPU times of the real and complex solver.

Inspection of Tables II and III reveals the greater efficiency of the complex solver with S_s in the range $2.6 \div 4.9$. The overall cost of the complex solver is markedly less than that of the real solver because both IC and IT are smaller. Note that while IC is not sensitive to k, IT also depends on k, as is shown in Fig. 2 for the TFQMR solver. Figure 2 points out that IT vs k increases with the real solution approach while it is stable or slightly decreases with the complex solution approach. This is due to the fact that R_k grows with k and, correspondingly, the antisymmetric part G_A of the coefficient matrix of (9) tends to dominate over the symmetric part G_S. In fact it is

$$G_S = \frac{1}{2}\begin{pmatrix} G_R + G_R^T & \emptyset \\ \emptyset & G_R + G_R^T \end{pmatrix}$$

and

$$G_A = \frac{1}{2}\begin{pmatrix} G_R - G_R^T & -2S_I \\ 2S_I & G_R - G_R^T \end{pmatrix}$$

which shows that the off-diagonal blocks of G_A become more important when parameter p_k is in the upper k range. By contrast G_s is insensitive to p_k. An enhanced G_A deteriorates the quality of the incomplete triangular factorization ILU(0) of system (9), and hence the overall performance of the solver. By distinction, when the original complex system is solved with complex arithmetic, the preconditioning tends to be improved with increasing k. Actually

TABLE III
Performance of TFQMR (*T*) and Bi-CGSTAB (*B*) in the Solution of the Complex System (4) for Sample Problem 1

r	Solver	IT	IC(s)	CPUT(s)	S_s
16	T	160	0.015	2.4	3.1
16	B	165	0.015	2.5	2.6
32	T	301	0.015	4.6	3.7
32	B	281	0.015	4.4	3.3
64	T	533	0.016	8.3	4.9
64	B	481	0.016	7.6	4.5

Note. S_s indicates the average speed-up of the complex solver.

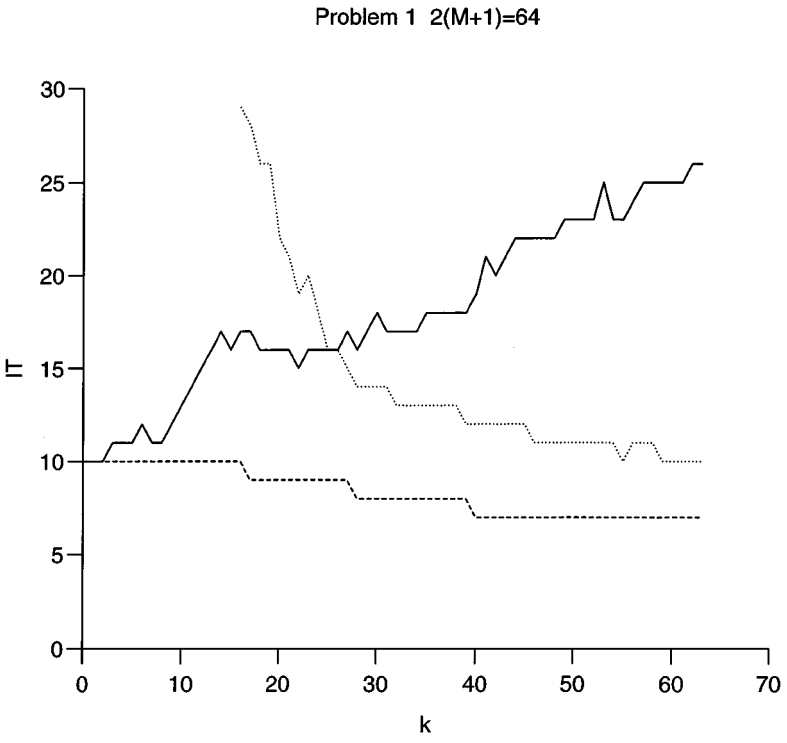

FIG. 2. Performance of TFQMR vs $p_k, k = 0, 1, \ldots, 63$, for sample Problem 1. (Solid line, real solver; dashed line, complex solver; dotted line, real solver with reordering.)

in the limit when the imaginary part S_I of S dominates, the incomplete factors of G are close to those of S_I which is a symmetric positive definite matrix. Experience shows that the incomplete factorization of such a matrix often represents an excellent preconditioner for a projection method of the kind discussed in the present analysis. Hence preconditioning of the complex solver improves for p_k moving from the lower part to the upper part in the interval of interest ($0 \leq k \leq 80$) of the Laplace parameter. The exact opposite occurs to preconditioning of the real solver. The previous findings are conceptually consistent with the results of the analysis performed in [12] which indicates that usually the transformation of a complex system to a real one has detrimental effects on convergence. The present study also provides a quantitative evaluation of the corresponding loss of efficiency in the FELT approach.

Careful inspection of G_A suggests, however, that a better preconditioning of the real matrix might be expected by properly reordering the columns of the coefficient matrix of Eq. (9). If G_R and S_I are simply permuted, and the same is done with $\bar{\mathbf{c}}_{m,R}$ and $\bar{\mathbf{c}}_{m,I}$ and the real and the imaginary parts of the know vector, the symmetric and antysimmetric parts of the reordered matrix read

$$G_S = \frac{1}{2}\begin{pmatrix} -2S_I & G_R + G_R^T \\ G_R + G_R^T & 2S_I \end{pmatrix}$$

and

$$G_A = \frac{1}{2}\begin{pmatrix} \emptyset & G_R - G_R^T \\ G_R - G_R^T & \emptyset \end{pmatrix}.$$

TABLE IV
The Same as Table II for Sample Problem 2

r	Solver	IT(s)	IC(s)	CPUT(s)
16	T	380	0.12	47.3
16	B	322	0.12	39.7
32	T	1341	0.12	158.2
32	B	1181	0.12	136.0
64	T	3913	0.12	451.1
64	B	3507	0.11	392.2

The above equations indicate that now G_A does not grow further with k while G_S becomes more important for larger k. According to [11] the sparsity pattern of a matrix, and hence reordering, may affect the quality of the ILU(0) preconditioner. Figure 2 shows the new real solver performance after the above reordering. Notice that IT decreases as k increases. However, IT for the initial reordered system ($k = 0$) is much larger than it is for the original non-reordered matrix. The break-even point occurs at $k = 25$. Reordering yields a higher solver performance for k in the upper range but a slower convergence for the initial k-values. On balance the performance of the real solver on the whole k-spectrum remains almost unchanged and the marked superiority of the complex solver is reconfirmed for the FELT method as a whole.

4.2. *Sample Problem* 2: *Two Dimensional Transport with Uniform Velocity*

The second problem addresses a square domain of 100×100 m, with a uniform velocity field from left to right: $v_x = 0.05$ m/day, $v_y = 0$. Dirichlet boundary conditions $c_m = 1$ are prescribed on the left, and no contaminant flux condition on the other sides of the domain. Other parameters of simulation are $\alpha_L = 0.033333$ m, $\alpha_T = 0.0033333$ m, $T_m = T_{im} = 0.2$, $\alpha = 0.005$ day^{-1}, and $\lambda = 0$. The domain is discretized with 61 nodes on each side for a total of $N = 3721$ nodes and 7200 triangular elements. P_e turns out to be equal to 500, so the problem is highly advection dominated. The maximum simulation time is $t_{max} = 150$ days. The real linear system has dimension $2N = 7442$ with 25,561 nonzero coefficients. The performances of TFQMR and Bi-CGSTAB are shown in Tables IV and V for the real and complex solution approaches, respectively.

The behavior of the TFQMR solver against the Laplace parameter is shown in Fig. 3 which points out an outcome similar to the one of Fig. 2 with a larger quantitative difference,

TABLE V
The Same as Table III for Sample Problem 2

r	Solver	IT	IC(s)	CPUT(s)	S_s
16	T	208	0.057	11.9	4.0
16	B	217	0.055	12.0	3.3
32	T	337	0.059	19.8	8.0
32	B	333	0.057	19.1	7.1
64	T	544	0.061	33.3	13.5
64	B	503	0.061	30.5	12.9

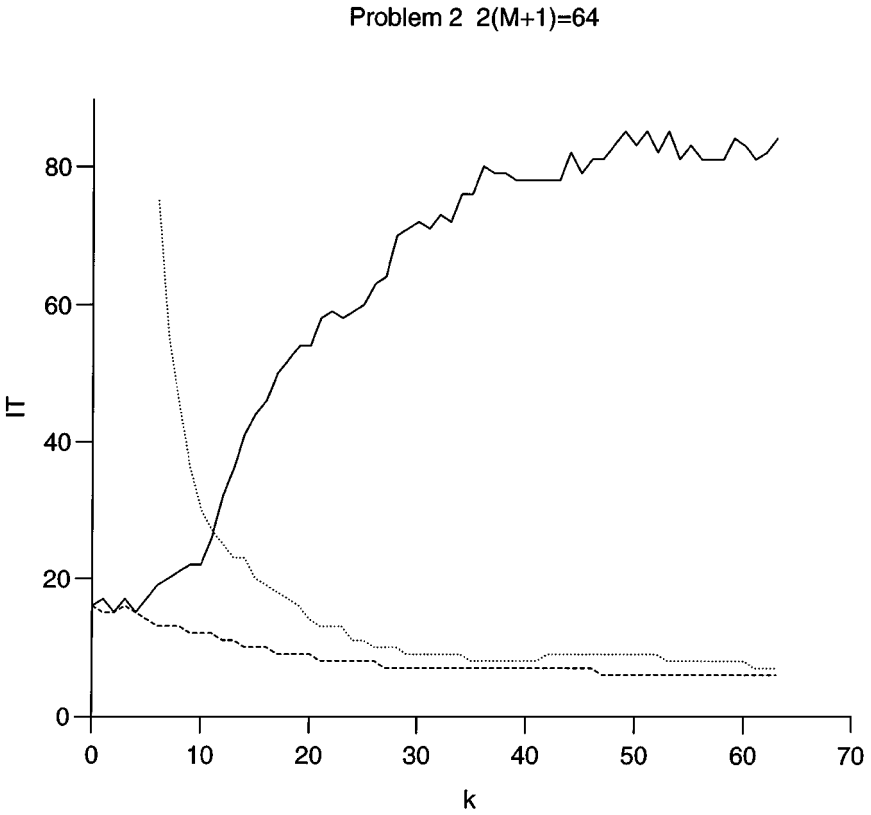

FIG. 3. The same as Fig. 2 for sample Problem 2.

however, between the real and the complex solver. The break-even point of the original and reordered solvers is observed for $k = 11$. For this example we have $\Upsilon_k = 1.14\ 10^{-3} + 2.74\ 10^{-5}k^2$; $Z_k = 2.88\ 10^{-2}\Upsilon_k + 4.86\ 10^{-6} + 1.37\ 10^{-7}k^2$, and

$$R_k = \frac{6.11\ 10^{-6}k + 1.44\ 10^{-7}k^3}{3.7\ 10^{-5} + 9.29\ 10^{-7}k^2}.$$

The R_k expression shows that R_k grows approximately linearly with k with high R_k values occurring for k in the upper range (Table I), and this accounts for the pronounced difference in the solid and dashed profiles of Fig. 3 and the high speed-ups achieved for r in the upper k range (Table V).

4.3. *Sample Problem* 3: *Two-Dimensional Transport with Non-uniform Velocity*

The last sample problem is adapted from [20], and involves transport in a ditch drained aquifer with a steady rainfall and infiltration of a reactive contaminant. The steady velocity field is computed in [17] and is not uniform. The values of the main simulation parameters are given in Table VI. The domain is discretized using $N = 15{,}275$ nodes and 29,952 elements. Linear real systems of size $2N = 30{,}550$ with 105,727 nonzero coefficients are thus obtained. The results of TFQMR and Bi-CGSTAB are shown in Tables VII and VIII for the real solver and in Tables IX and X for the complex solver. Inspection of these tables

TABLE VI
Main Parameters of Sample Problem 3

Problem	α_L(m)	α_T(m)	T_m	T_{im}	α(day^{-1})	P_e	t_{max}(day)
3a	0.66667	0.66667	0.6	0.2	1	3	150
3b	1.	1.	0.6	0.2	1	2	150
3c	10^{-1}	10^{-2}	0.2	0.2	10^{-5}	20	6
3d	10^{-1}	10^{-2}	0.2	0.2	10^{-5}	20	21

TABLE VII
The Same as Table II for Sample Problems 3a and 3b

		Problem 3a			Problem 3b		
r	Solver	IT	IC(s)	CPUT(s)	IT	IC(s)	CPUT(s)
16	T	602	0.49	297.6	767	0.49	371.9
16	B	392	0.52	205.0	474	0.50	237.3
32	T	1169	0.49	579.2	1326	0.49	649.3
32	B	631	0.53	337.2	741	0.52	381.4
64	T	2927	0.49	1424.6	2838	0.49	1383.1
64	B	1390	0.53	729.4	1223	0.53	646.2

TABLE VIII
The Same as Table II for Sample Problems 3c and 3d

		Problem 3c			Problem 3d		
r	Solver	IT	IC(s)	CPUT(s)	IT	IC(s)	CPUT(s)
16	T	127	0.65	82.0	636	0.49	311.4
16	B	88	0.73	64.2	478	0.49	233.5
32	T	309	0.61	189.3	2015	0.48	959.8
32	B	209	0.67	140.9	1136	0.48	545.7
64	T	11921*	0.46	5557.9	23715*	0.46	10820.2
64	B	11421*	0.45	5184.3	9035*	0.46	4147.1

* No convergence within 1000 iterations for some p_k.

TABLE IX
The Same as Table III for Sample Problems 3a and 3b

		Problem 3a				Problem 3b			
r	Solver	IT	IC(s)	CPUT(s)	S_s	IT	IC(s)	CPUT(s)	S_s
16	T	538	0.20	109.9	2.7	651	0.20	132.1	2.8
16	B	931	0.19	181.0	1.1	917	0.20	179.5	1.3
32	T	734	0.21	153.8	3.8	908	0.21	188.1	3.5
32	B	1105	0.20	220.1	1.5	1380	0.20	272.2	1.4
64	T	1014	0.22	219.3	6.5	1232	0.21	263.2	5.3
64	B	1336	0.21	276.1	2.6	1650	0.20	335.4	1.9

TABLE X
The Same as Table III for Sample Problems 3c and 3d

		Problem 3c				Problem 3d			
r	Solver	IT	IC(s)	CPUT(s)	S_s	IT	IC(s)	CPUT(s)	S_s
16	T	97	0.26	25.0	3.3	270	0.22	58.6	5.3
16	B	73	0.28	20.1	3.2	248	0.21	53.0	4.4
32	T	193	0.26	49.8	3.8	400	0.23	90.0	10.7
32	B	137	0.28	38.5	3.7	357	0.22	79.7	6.8
64	T	385	0.26	99.3	56.0	612	0.23	143.5	75.4
64	B	265	0.28	75.2	68.9	517	0.24	122.4	33.9

points out that in most cases Bi-CGSTAB is faster than TFQMR in the solution of both the real and the complex systems while the speed-up S_s for the complex TFQMR is generally higher.

Notice that the performance of TFQMR and Bi-CGSTAB becomes closer in complex arithmetic. Particularly instructive are the results of sample Problems 3c and 3d which indicate that the real solvers converge very slowly, or even fail to converge, for p_k values in the upper k range. By contrast, the complex solver converges quite fast over the entire k interval. This is consistent with similar results from sample Problems 1 and 2, and already commented on, and with the R_k behavior of Table I. Figure 4 gives the iterations required by

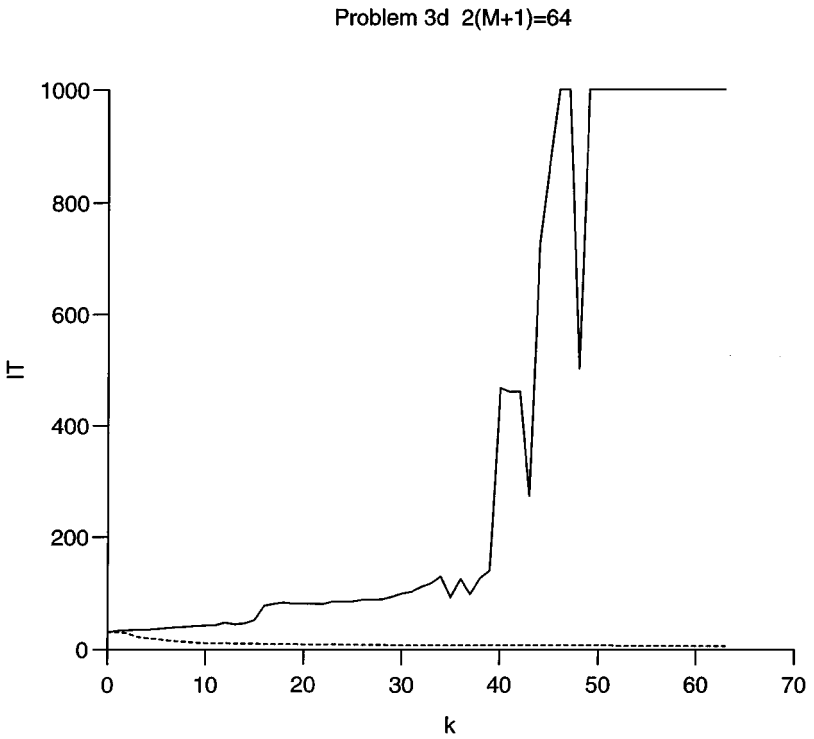

FIG. 4. Performance of TFQMR vs $p_k, k = 0, 1, \ldots, 63$, for sample Problem 3d. (Solid line, real solver; dashed line, complex solver.)

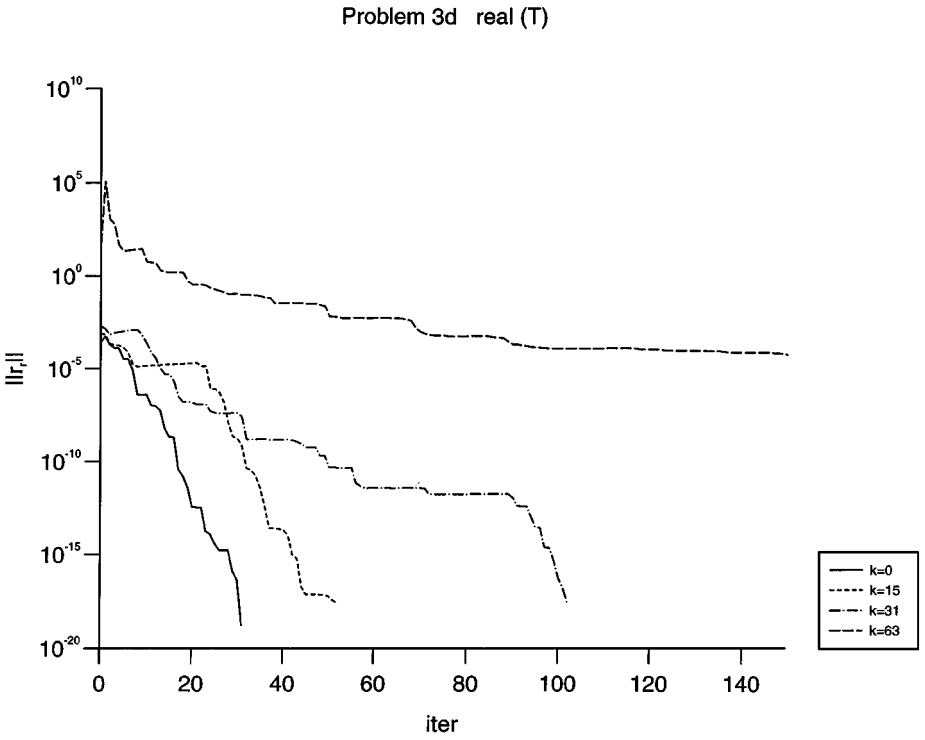

FIG. 5. Convergence profile of the original real solver for sample Problem 3d.

TFQMR in the solution of the real and complex systems against p_k for sample Problem 3d. Because the break-even point occurs at a k-value larger than 63, the profile showing the performance of the real solver with reordering is not plotted in Fig. 4. This result, together with the others already discussed, reveals that the break-even point of the real (reordered) solver is very much problem dependent while the superiority of the complex solver is problem independent. As experimented with in the previous examples, the performance of the complex solver increases for larger k when the imaginary part of the complex matrix becomes more dominant. By distinction the real TFQMR without reordering behaves much worse, and particularly so in Problems 3c and 3d where P_e is high and the mass transfer coefficient is small. Finally, as an example, Figs. 5 and 6 show selected convergence profiles of the real and complex solver, respectively, for sample Problem 3d. Again observe the opposite behavior of the solver vs k. While the convergence rate of the complex solver increases greatly for the highest k-values, the convergence of the real one displays a pronounced reduction, and even a stagnation at $k = 63$. Permuting the columns of the real matrix as suggested in Subsection 5.1 overall yields no improvement for this example.

5. CONCLUSION

The FELT approach for the integration of nonequilibrium or nonideal solute transport in porous media requires the solution of several linear complex valued equations with different coefficient matrices and known vectors. These sets of equations can be solved either in the complex space by direct use of complex arithmetic or in the real space by defining an equivalent real system twice as large. In both spaces the preconditioned conjugate gradient-

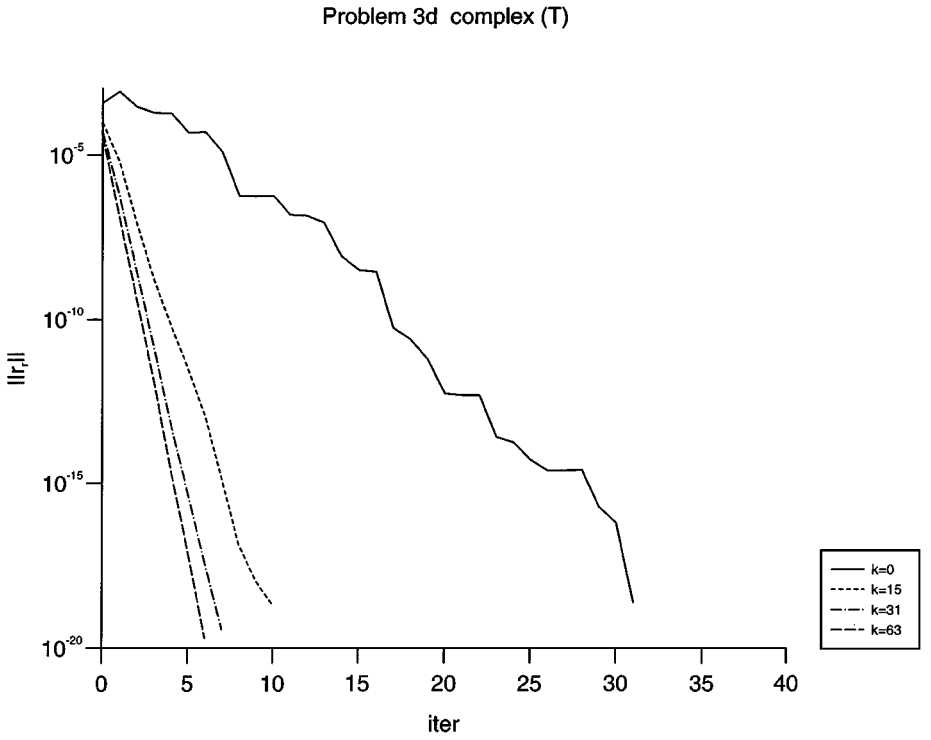

FIG. 6. Convergence profile of the complex solver for sample Problem 3d.

like methods TFQMR and Bi-CGSTAB have been used. The results show that the complex solver outperforms the real one by a factor S_s which for TFQMR can be as large as 75, according to the problem, with an average value of the order of 10. Reordering the real equations may induce a significant change in the local solver performance with, however, no significant global improvement over the entire p_k range, i.e., in the FELT method as a whole. Similarly complex Bi-CGSTAB is superior to real Bi-CGSTAB, although slightly less than TFQMR. For particularly difficult advection dominated problems the real solver may even fail to converge while the complex solver is always successful. Therefore the projection methods relying on complex arithmetic appear to be both a cost-effective and a robust tool for the solution of nonequilibrium or nonideal transport equation by the finite element Laplace transform approach.

ACKNOWLEDGMENTS

This work has been supported in part by Fondi Ministeriali MURST 40% (cofinanziamento) and by INCO-COPERNICUS program of the European Community (Contract ERBIC15CT960211).

REFERENCES

1. M. B. Allen III, I. Herrera, and G. F. Pinder, *Numerical Modeling in Science and Engineering* (Wiley, New York, 1988).
2. E. Barragy, G. F. Carey, and R. A. Walters, Application of conjugate gradient methods to tidal simulation, *Adv. Water Resources* **16**, 163 (1993).

3. J. Bear, *Hydraulics of Groundwater* (McGraw–Hill, New York, 1979).
4. W. E. Boyse and A. A. Seidl, A block QMR method for computing multiple simultaneous solutions to complex symmetric systems, *SIAM J. Sci. Comput.* **17**(1), 263 (1996).
5. M. L. Brusseau and P. S. C. Rao, Sorption nonideality during organic contaminant transport in porous media, *Crit. Rev. Env. Contr.* **19**(1), 33 (1989).
6. M. L. Brusseau, Transport of reactive contaminants in heterogeneous porous media, *Rev. Geophys.* **32**(3), 285 (1994).
7. M. Clemens and T. Weiland, Iterative methods for the solution of very large complex symmetric linear systems of equations in electrodynamics, preprint, Multigrid Copper Mountain 96.
8. K. S. Crump, Numerical inversion of Laplace transforms using a Fourier series approximation, *J. Assoc. Comput. Mach.* **23**, 89 (1976).
9. S. K. Datta, S. Liu, and T. Ju, The application of the Conjugate Gradient method to large sparse unsymmetric complex matrix equations arising from the scattering of elastic waves, paper presented at Copper Mountain Conference on Iterative Methods, Copper Mountain, CO, April 1990.
10. F. R. de Hoog, J. H. Knight, and A. N. Stokes, An improved method for numerical inversion of Laplace transforms, *SIAM J. Sci. Stat. Comput.* **3**(3), 357 (1982).
11. I. S. Duff and G. Meurant, The effect of ordering on preconditioned conjugate gradients, *BIT* **29**, 635 (1989).
12. R. W. Freund, Conjugate gradient type methods for linear systems with complex symmetric coefficient matrices, *SIAM J. Sci. Stat. Comput.* **13**, 425 (1992).
13. R. W. Freund, A transpose-free quasi-minimal residual algorithm for non-Hermitian linear systems, *SIAM J. Sci. Comput.* **14**, 470 (1993).
14. C. Gallo, C. Paniconi, and G. Gambolati, Comparison of solution approaches for the two-domain model of nonequilibrium transport in porous media, *Adv. Water Resources* **19**(4), 241 (1996).
15. G. Gambolati, C. Paniconi, and M. Putti, Mass transfer analysis in sorbing porous media by an integro-differential approach, in *Advances in Hydro-Science and Engineering*, edited by S. S. Y. Wang (University, MS, The University of Mississippi, 1993), Vol. I, Part B, p. 1819.
16. G. Gambolati, C. Gallo, and C. Paniconi, *Numerical integration methods for the dual porosity model in sorbing porous media*, in *Computational Methods in Water Resources X*, edited by A. Peter *et al.* (Kluwer Academic, Dordrecht, 1994), Vol. 1, p. 621.
17. G. Gambolati, G. Pini, M. Putti, and C. Paniconi, Finite element modeling of the transport of reactive contaminants in variably saturated soils with LEA and non-LEA sorption, in *Environmental Modeling II*, edited by P. Zannetti (Computational Mechanics Publications, Southampton, UK, 1994), p. 173.
18. G. Gambolati, M. Putti, and C. Paniconi, Projection methods for the finite element solution of the dual-porosity model in variably saturated porous media, in *Recent Advances in Ground-Water Pollution Control and Remediation*, edited by M. M. Aral, NATO ASI Series G: Ecological Sciences (Kluwer Academic, Dordrecht, 1996), p. 97.
19. G. Gambolati, C. Gallo, C. Paniconi, and M. Putti, Numerical solutions for nonequilibrium solute transport in porous media, in *Advances in Hydro-Science and Engineering* (Tsinghua University Press, Beijing, China, 1995), Vol. II, Part B, p. 1733.
20. A. B. Gureghian, *TRIPM, a Two-Dimensional Finite Element Model for the Simultaneous Transport of Water and Reacting Solutes through Saturated and Unsaturated Porous Media*, Technical Report ONWI-465, Off. of Nuclear Water Isolation, Columbus, OH, 1983.
21. P. Joly and G. Meurant, Complex conjugate gradient methods, *Numer. Alg.* **4**, 379 (1993).
22. D. S. Kershaw, The incomplete Cholesky-conjugate gradient method for the iterative solution of systems of linear equations, *J. Comput. Phys.* **26**, 43 (1978).
23. C. Lanczos, Solution of systems of linear equations by minimized iterations, *J. Res. Natl. Bur. Standard* **49**, 33 (1952).
24. H. M. Leismann, B. Herrling, and V. Krenn, A quick algorithm for the deadend pore concept for modeling large-scale propagation processes in groundwater, in *Numerical Methods for Transport and Hydrologic Processes*, edited by M. A. Celia *et al.* (Elsevier, Amsterdam, Holland, 1988), Vol. 2, p. 275.
25. J. A. Meijerink and H. A. van der Vorst, An iterative solution method for linear systems of which the coefficient matrix is a symmetric M-matrix, *Math. Comput.* **31**, 148 (1977).

26. G. Pini and M. Putti, Parallel finite element Laplace transform method for the non-equilibrium groundwater transport equation, *Int. J. Numer. Methods Eng.* **40**, 2653 (1997).
27. Y. Saad, *Iterative Methods for Sparse Linear Systems* (PWS, Boston, 1996).
28. R. Sauter, The finite element method and ILU preconditioners, *J. Comput. Appl. Math.* **36**(1), 91 (1991).
29. E. A. Sudicky, The Laplace transform Galerkin technique: A time-continuous finite element theory and application to mass transport in groundwater, *Water Resour. Res.* **25**(4), 1833 (1989).
30. E. A. Sudicky, The Laplace transform Galerkin technique for efficient time-continuous solution of solute transport in double-porosity media, *Geoderma* **46**, 209 (1990).
31. H. A. van der Vorst, Bi-CGSTAB: A fast and smoothly converging variant of BI-CG for the solution of nonsymmetric linear systems, *SIAM J. Sci. Stat. Comput.* **13**, 631 (1992).
32. R. Wait and A. R. Mitchell, *Finite Element Analysis and Applications* (Wiley, New York, 1985).
33. W. J. Weber, Jr., P. McGinley, and L. Katz, Sorption phenomena in subsurface systems: Concepts, models and effects on contaminant fate and transport, *Water Res.* **25**(5), 499 (1991).
34. O. C. Zienkiewicz and R. L. Taylor, *The Finite Element Method* (McGraw–Hill, New York, 1989), 4th ed., Vols. 1, 2.